

Article

Not peer-reviewed version

Probabilistic Modeling of Urban Vehicle Traffic Under COVID-19 Mobility Restrictions Using AI-Based Video Data: A Case Study in Cluj-Napoca

[Nicolae Filip](#), [Calin Iclodean](#)^{*}, [Marius Deac](#)

Posted Date: 26 February 2026

doi: 10.20944/preprints202602.1697.v1

Keywords: COVID-19 pandemic; urban traffic flow; probability estimation; poisson distribution; smart mobility



Preprints.org is a free multidisciplinary platform providing preprint service that is dedicated to making early versions of research outputs permanently available and citable. Preprints posted at Preprints.org appear in Web of Science, Crossref, Google Scholar, Scilit, Europe PMC.

Copyright: This open access article is published under a [Creative Commons CC BY 4.0 license](#), which permit the free download, distribution, and reuse, provided that the author and preprint are cited in any reuse.

Disclaimer/Publisher's Note: The statements, opinions, and data contained in all publications are solely those of the individual author(s) and contributor(s) and not of MDPI and/or the editor(s). MDPI and/or the editor(s) disclaim responsibility for any injury to people or property resulting from any ideas, methods, instructions, or products referred to in the content.

Article

Probabilistic Modeling of Urban Vehicle Traffic Under COVID-19 Mobility Restrictions Using AI-Based Video Data: A Case Study in Cluj-Napoca

Nicolae Filip, Calin Iclodean * and Marius Deac

Department of Automotive Engineering and Transports, Technical University of Cluj-Napoca Romania, Muncii Bd. 103-105, 400114 Cluj-Napoca, Romania

* Correspondence: calin.iclodean@auto.utcluj.ro

Abstract

The COVID-19 pandemic and the resulting mobility restrictions significantly disrupted urban traffic patterns. This study quantitatively assesses the impact of these restrictions on vehicle flow at a signalized central intersection in Cluj-Napoca, Romania, through an integrated methodology combining continuous radar-based traffic measurements and AI-assisted video analysis. Traffic data were collected before the pandemic (November 2019) and during the lockdown period (April 2020), enabling a comparative evaluation of flow characteristics and vehicle arrival patterns. Under constrained observational conditions, vehicle arrivals were modeled using a probabilistic framework grounded in the Poisson distribution. The findings indicate a dramatic contraction of mobility demand, with traffic volumes declining in 2020 to 9.55% of pre-pandemic levels. The probabilistic assessment highlights the predominance of free-flow regimes under reduced demand and confirms the adequacy of the Poisson model in low-density traffic scenarios. The proposed framework is transferable to other urban contexts and supports resilience-oriented, data-driven traffic management under extreme mobility disruptions.

Keywords: COVID-19 pandemic; urban traffic flow; probability estimation; poisson distribution; smart mobility

1. Introduction

Urban mobility systems are characterized by continuous growth in travel demand and increasing pressure on road infrastructure, facing major challenges such as climate change associated with transport-related emissions, deterioration of urban quality of life, and prolonged daily travel times [1]. From an engineering perspective, these challenges are directly reflected in traffic flow dynamics, congestion levels, and the operational performance of traffic control systems.

The global spread of SARS-CoV-2 (COVID-19) in early 2020 led to the implementation of unprecedented mobility restrictions worldwide [2–4]. These measures caused an abrupt contraction in vehicular travel demand, creating a natural experimental setting for examining traffic flow behavior under low-demand conditions.

Traffic congestion generates substantial economic losses and adversely affects the efficiency of urban transport systems. Urban mobility is a key determinant of economic competitiveness [5–7]. From a traffic modeling standpoint, significant demand fluctuations provide an opportunity to assess the robustness and validity of statistical models commonly used for vehicle arrival estimation.

Ensuring sustainable, reliable, and efficient urban mobility requires the implementation of strategic planning instruments such as Sustainable Urban Mobility Plans (SUMP), which rely on quantitative traffic analysis and predictive modeling approaches [8–10]. In this context, evaluating the statistical distribution of vehicle arrivals under atypical operating conditions becomes particularly relevant for calibrating and validating probabilistic traffic models.

This study investigates daytime vehicular traffic dynamics in Cluj-Napoca, Romania, employing the Poisson distribution as the primary modeling framework. The main objective is to estimate and compare vehicle arrival distributions before and during the lockdown period, based on traffic data collected in November 2019 and April 2020. The research focuses on short time-interval flow variations, the suitability of the Poisson distribution for modeling low-demand traffic regimes, and the quantitative assessment of traffic reduction relative to baseline conditions.

In Romania, a state of emergency was declared on 16 March 2020 through Decree No. 195 [11], introducing strict mobility restrictions. These measures resulted in a rapid and significant decline in traffic volumes.

At the global level, mobility reduction during the pandemic was associated with an estimated 5.4% decrease in greenhouse gas emissions in 2020 [12–15]. This reduction is directly linked to lower vehicular traffic volumes, highlighting the importance of accurately quantifying traffic flows during large-scale disruptions.

By integrating radar-based traffic measurements, AI-assisted video analysis, and probabilistic modeling, this paper proposes a methodological framework for assessing vehicular traffic behavior under extreme mobility conditions.

2. Literature Review

International studies conducted between 2020 and 2022 consistently reported substantial reductions in urban mobility following the implementation of COVID-19-related restrictions. Most research documented significant declines in both public transport usage and private vehicular traffic volumes.

El-Geneidy et al. [16] reported reductions of 80–90% in public transport ridership in countries with strict mobility restrictions. Similar analyses conducted across Europe, Asia, and North America indicated traffic volume reductions ranging from 50% to 90% during the initial months of the pandemic [17–26].

From a vehicular traffic perspective, the literature highlights:

- Decreases in traffic intensity of up to 70% at urban intersections [22].
- Increases in average travel speeds under low-demand conditions [26].
- Structural shifts in modal distribution and temporal travel patterns [18–23].

These findings confirm that the pandemic period generated an atypical traffic regime characterized by low demand levels and significant modifications in flow dynamics.

Beyond descriptive analyses of mobility reduction, several studies have investigated the statistical properties of vehicle arrivals using probabilistic models, particularly the Poisson distribution [30]. The Poisson framework is widely applied to model independent vehicle arrivals over short time intervals and is generally considered appropriate for low- to moderate-density traffic conditions.

Peköz et al. [31] employed the Poisson distribution to estimate traffic flow within a stationary ergodic intersection model. Abul-Magd et al. [32] used a Poisson-based approach to analyze the transition from free-flow to congested traffic regimes. The analytical formulation of inter-vehicle spacing and time-headway distributions has also been derived using Poisson assumptions combined with Wigner's Surmise [33].

Maya et al. [34] proposed a bilinear and convolutional Poisson-based framework for multi-segment traffic flow estimation, integrating machine learning algorithms and stochastic variational Bayesian techniques to enable real-time parameter updates. Yang et al. [35] developed a Poisson-based analytical model for vehicle platoon behavior at signalized intersections. Thomas et al. [36] demonstrated that seasonal traffic noise variability followed a Poisson distribution in Almelo, the Netherlands.

Additional applications include queue delay evaluation and signal timing optimization based on Poisson assumptions [37], intersection transit-time modeling [38], and congestion anticipation using vehicle trajectory data weighted within a Poisson-based framework [39].

However, most of these studies were conducted under normal operating conditions or focused primarily on congestion analysis. Limited research has addressed extreme low-demand regimes induced by large-scale mobility restrictions.

Current literature reveals a significant gap in:

1. Validating the Poisson distribution under severely reduced urban traffic conditions characterized by fluctuating demand and atypical flow behavior.
2. Robustly estimating vehicle arrival distributions based on limited datasets collected during large-scale disruptions.
3. Integrating continuous radar-based traffic measurements with AI-assisted trajectory extraction to develop probabilistic models capable of adapting to dynamic urban contexts.

Few studies combine multisensory data acquisition (radar and video), artificial intelligence-based vehicle detection, and probabilistic modeling within a unified framework for analyzing lockdown traffic conditions.

3. Materials and Methods

3.1. Traffic Data Collection Methodology

3.1.1. Fixed Traffic Surveillance Camera

To analyze vehicular traffic behavior before and during the COVID-19 pandemic, two complementary data acquisition methods were employed:

1. Continuous cross-sectional traffic measurements and
2. Video-based analysis using fixed surveillance cameras.

The video monitoring system (Figure 1) consists of fixed cameras installed at the analyzed intersection and integrated into the municipal traffic management system.



Figure 1. Fixed traffic surveillance camera (photo by the author).

The deployed cameras enable continuous intersection-level monitoring, providing detailed information on vehicle trajectories, vehicle classification, and kinematic parameters such as instantaneous speed and estimated acceleration. The analyzed video recordings were collected

during two distinct periods: November 2019 (representing normal traffic conditions) and April 2020 (corresponding to the lockdown period).

Subsequently, the video data were processed to detect and classify moving objects (vehicles and pedestrians) and to extract relevant traffic parameters, as described in the following subsection.

The surveillance cameras form part of the urban traffic management infrastructure [8], which includes adaptive signal control systems and traffic sensors. This integration ensures consistency between video-derived data and operational traffic control parameters, facilitating a comprehensive analysis of vehicular flow dynamics.

3.1.2. Continuous Traffic Measurements

To evaluate macroscopic traffic parameters, namely vehicle flow and average travel speed, an automatic radar-based detection system (Speed Detection Radar – SDR Data Collect) was employed (Figure 2) [40].

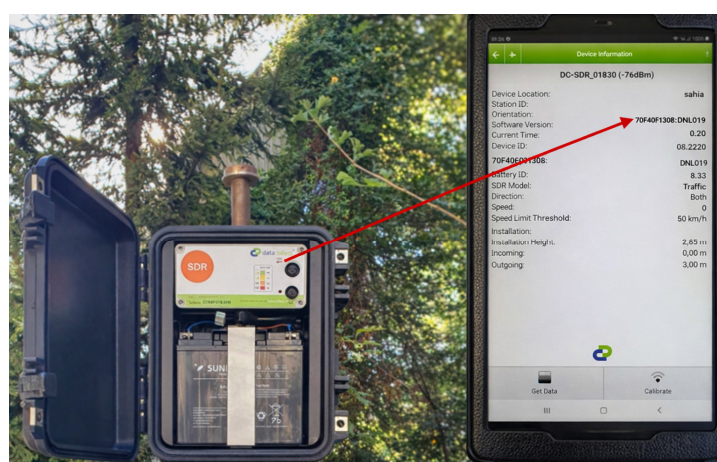


Figure 2. Vehicle detecting equipment SDR (photo by the author).

The SDR Data Collect device operates using microwave radar technology at a frequency of 24.125 GHz and determines the speed of moving objects based on the Doppler effect principle [40,42]. The Doppler effect occurs when the device emits an electromagnetic wave toward a moving object and the reflected wave returns to the radar sensor with a frequency shift proportional to the relative velocity (Figure 3).

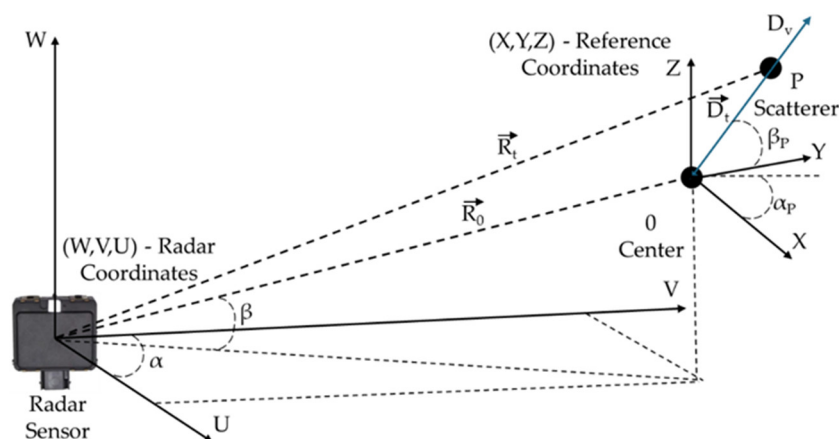


Figure 3. Operating principle of SDR Data Collect based on the radar Doppler effect.

Within the experimental framework, the SDR unit was installed in a cross-sectional configuration relative to the direction of travel and operated continuously (24 h/day) for seven consecutive days in November 2019 and seven consecutive days in April 2020.

The dataset collected included:

- the number of vehicles detected within predefined time intervals,
- the instantaneous speed of each detected vehicle,
- and the direction of travel.

These measurements enabled a quantitative and dynamic characterization of traffic flow conditions [43,44].

The main technical characteristics of the SDR Data Collect system are summarized in Table 1 [41].

Table 1. Technical specifications of the SDR Data Collect system.

| Specification | Unit | Value |
|-----------------------|------|---------------|
| Sensor type | - | Microwave |
| Frequency | GHz | 24.125 |
| Speed measuring range | km/h | 3.00 – 199.00 |
| Speed resolution | km/h | 1.00 |
| Distance resolution | m | 0.10 |
| Data rate | baud | 115200 |
| Power | mW | 5.00 |

The Doppler frequency shift f_D depends on the electromagnetic wavelength λ and the relative velocity V between the radar sensor and the moving target. It can be expressed as [45]:

$$\begin{aligned}
 f_D &= \frac{1}{2\pi} \frac{d\phi(t)}{dt} = \frac{2f}{c} \frac{d}{dt} r(t) = \frac{2f}{c} \frac{1}{2r(t)} \left[(\vec{R}_0 + \vec{V}_t + \mathfrak{R}_t \vec{r}_0)^T (\vec{R}_0 + \vec{V}_t + \mathfrak{R}_t \vec{r}_0) \right] \\
 &= \frac{2f}{c} \left[\vec{V} + \frac{d}{dt} (\mathfrak{R}_t \vec{r}_0) \right]^T \vec{n} = \frac{2f}{c} \left[\vec{V} + \frac{d}{dt} (e^{\hat{\omega}t} \vec{r}_0) \right]^T \vec{n} \\
 &= \frac{2f}{c} (\vec{V} + \hat{\omega} e^{\hat{\omega}t} \vec{r}_0)^T \vec{n} = \frac{2f}{c} (\vec{V} + \hat{\omega} \times \vec{r})^T \vec{n}
 \end{aligned} \tag{1}$$

The phase of the baseband signal $\Phi[r(t)]$ is defined as:

$$\Phi[r(t)] = 2\pi f \frac{2r(t)}{c} \tag{2}$$

The unit vector \vec{n} representing the direction from the radar sensor to the target is defined as:

$$\vec{n} = (\vec{R}_0 + \vec{V}_t + \mathfrak{R}_t \vec{r}_0)^T / (\|\vec{R}_0 + \vec{V}_t + \mathfrak{R}_t \vec{r}_0\|) \tag{3}$$

where: f is the carrier frequency, c is the speed of the electromagnetic wave propagation, $\vec{r} = \vec{r}_0 + \vec{r}'$ represents the initial coordinates of the target in the radar coordinate system (U,V,W), \vec{r}_0 is the translation vector, respectively \vec{r}' represents the coordinates of the target after translation (U₁,V₁,W₁), \vec{R}_0 is the distance from the radar sensor to the reference coordinate system (X,Y,Z), \vec{V} is the translation velocity, \vec{V}_t is the translation velocity at the time t, $\mathfrak{R}_t = \exp\{\hat{\omega}t\}$ denotes the rotation matrix, and $e^{\hat{\omega}t}$ denotes the skew-symmetric matrix.

These formulations describe the relationship between phase variation and relative motion, enabling velocity estimation through Doppler shift analysis.

The SDR system was configured using the dedicated myTrafficData application [46], which enables parameter setting, real-time monitoring, and cloud-based data storage (Figure 4).

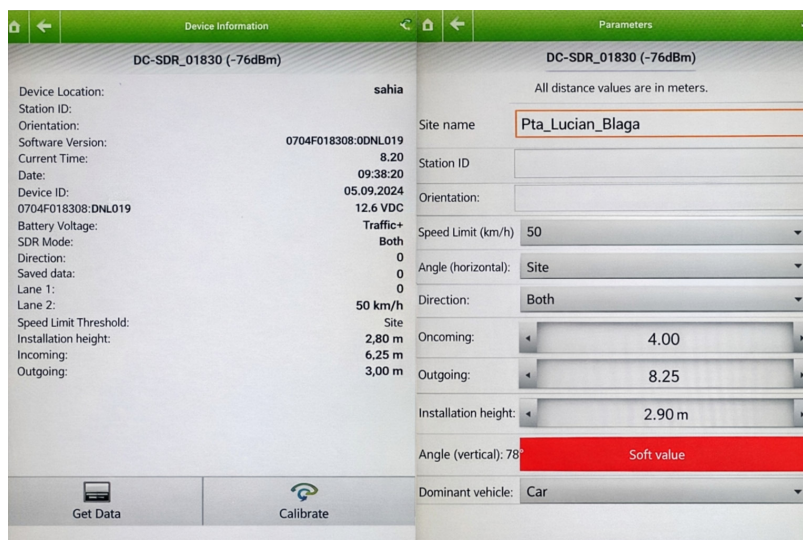


Figure 4. myTrafficData application interface and SDR Data Collect device (photo by the author).

Calibration of the detection geometry was performed by correlating the radar position with the roadway cross-section geometry to minimize measurement errors. The device was installed at a horizontal angle of 45° relative to the longitudinal axis of the roadway and a vertical angle of 78° , resulting in an elliptical detection zone aligned with the monitored traffic section.

The 45° horizontal configuration enables longitudinal velocity estimation through cosine correction of the Doppler component, ensuring accurate measurement of vehicle speed along the travel direction.

3.1.3. Traffic Measurements Using Image Processing

Following radar-based data acquisition, the video recordings obtained from the fixed surveillance cameras were processed using the Data From Sky (DFS) platform (Figure 5) [47–50].

The DFS platform enables automated object detection and tracking in video sequences through deep learning algorithms based on convolutional neural networks (CNNs). In the present study, only recordings from fixed cameras were used (LIGHT module), without employing aerial imagery.



Figure 5. Traffic detection using Data From Sky (photo by the author).

Video processing allowed object-level extraction of a comprehensive set of traffic-related parameters, including spatial position in each frame, full movement trajectory, vehicle classification, estimated speed, estimated acceleration, and total traversal time within the monitored area. The processed data were exported as compressed Tracking Log files containing frame-level information for each detected object, thereby supporting subsequent quantitative analysis and advanced statistical modeling (Figure 6) [50].

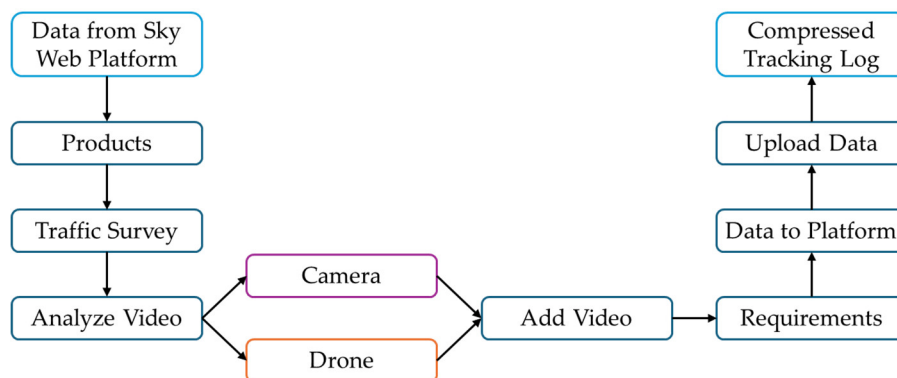


Figure 6. Functional block diagram of the Data From Sky platform.

The video data processing pipeline consisted of two main stages:

1. Georegistration, involving the establishment of correspondence between image pixels and real-world coordinates using fixed infrastructural reference points.
2. Object detection and tracking, comprising identification, classification, and trajectory monitoring of vehicles within the analyzed sequences.

The georegistration process enabled the transformation of image-space coordinates into metric spatial coordinates, ensuring accurate estimation of vehicle speed and travel distance, as well as consistency of derived kinematic parameters [51].

3.2. Research Methodology

The dataset obtained through radar-based measurements and AI-assisted video processing was used to analyze vehicle arrival distributions and to estimate traffic flow probabilities using the Poisson distribution framework. A comparative analysis was conducted for two distinct traffic regimes: (i) normal operating conditions (November 2019) and (ii) reduced-mobility conditions during the lockdown period (April 2020).

3.2.1. Case Study Site Description

The analyzed location was Lucian Blaga Square, situated in the central area of Cluj-Napoca, Romania (46°46'N, 23°35'E) [52]. The selected intersection represents a complex signalized urban node characterized by multiple entry and exit branches and significant temporal variability in vehicular demand.

The intersection is supplied by one three-lane arterial (Clinicilor Street) and three two-lane arterials (Victor Babeş Street, Petru Maior Street, and Gheorghe Şincai Street). Outbound traffic is distributed toward two two-lane arterials (Napoca Street and Republicii Street) and one single-lane branch (Petru Maior Street) (Figure 7).



Figure 7. The analyzed area (<https://cluj-city.map2web.eu/>).

The site was selected due to its operational relevance to the objectives of the study. It is classified as a recurrently congested urban node during peak hours and serves as a strategic connection between the main west–east and north–south corridors of the urban network. Its configuration enables the observation of transitions between congestion-prone and free-flow regimes under varying demand conditions, thereby providing an appropriate framework for assessing the validity of the Poisson distribution across distinct operational states [53].

The intersection operates under adaptive signal control integrated within the municipal traffic management system. This configuration generates a mixed traffic regime influenced both by vehicular demand and signal control logic. The presence of adaptive signalization is particularly relevant for arrival distribution analysis, as signal cycles may introduce temporal correlations between successive vehicles, potentially affecting the independence assumptions underlying Poisson-based modeling.

3.2.2. Traffic Measurements (Year 2019)

The measurements conducted in November 2019 were intended to characterize the normal operational regime of the analyzed intersection and to provide the reference dataset subsequently used for estimating the parameters of the Poisson distribution.

Raw data, consisting of individual vehicle detections [54] (Table 2), were aggregated into 15-minute intervals. This temporal resolution was selected to reduce random variability inherent in individual detections, ensure compatibility with typical signal cycle durations, and enhance the stability of the λ parameter estimation within the Poisson framework. Additionally, the chosen aggregation interval facilitated the identification of congestion-prone periods.

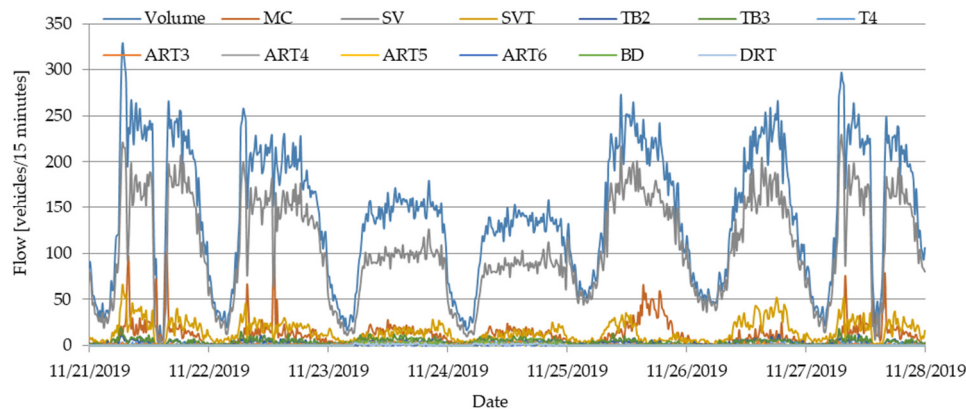
Table 2. Vehicle classification schemes (ARX).

| Class | Description | Parameters |
|-------|---|--|
| 1 MC | Very short (Bicycle, motorcycle) | $d(1) < 1.7\text{m}$ & axles=2 |
| 2 SV | Short (sedan, wagon, 4WD, utility, van) | $d(1) \geq 1.7\text{m}$, $d(1) \leq 3.2\text{m}$ & axles=2 |
| 3 SVT | Short towing (trailer, caravan) | groups=3, $d(1) \geq 2.1\text{m}$, $d(1) \leq 3.2\text{m}$, $d(2) \geq 2.1\text{m}$ & axles=3,4,5 |
| 4 TB2 | Two axle truck or bus | $d(1) > 3.2\text{m}$ & axles=2 |
| 5 TB3 | Three axle truck or bus | axles=3 & groups=2 |

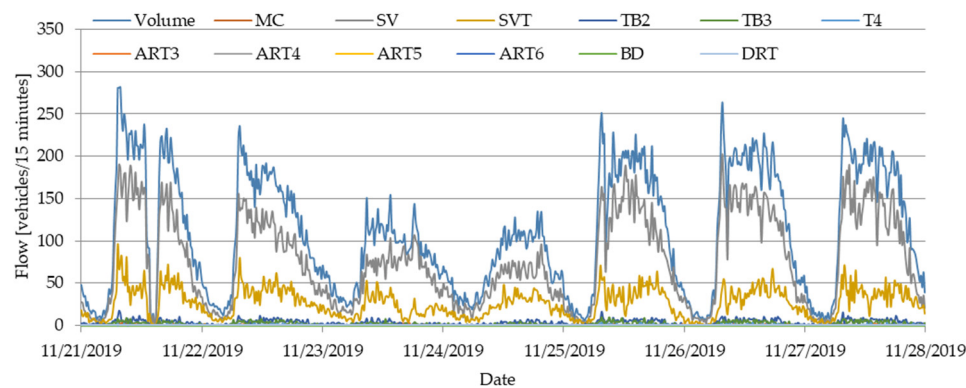
| | | | |
|----|------|---|---|
| 6 | T4 | Four axle truck | axles>3 & groups=2 |
| 7 | ART3 | Three axle articulated vehicle or rigid vehicle and trailer | d(1)>3.2m, axles=3 & groups=3 |
| 8 | ART4 | Four axle articulated vehicle or rigid vehicle and trailer | d(2)<2.1m or d(1)<2.1m or d(1)>3.2m axles = 4 & groups>2 |
| 9 | ART5 | Five axle articulated vehicle or rigid vehicle and trailer | d(2)<2.1m or d(1)<2.1m or d(1)>3.2m axles=5 & groups>2 |
| 10 | ART6 | Six (or more) axle articulated vehicle or rigid vehicle and trailer | axles=6 & groups>2 or axles>6 & groups=3 |
| 11 | BD | B-Double or heavy truck and trailer | groups=4 & axles>6 |
| 12 | DRT | Double or triple road train or heavy truck and two (or more) trailers | groups>=5 & axles>6 |

For each entry and exit branch (Figure 8 and Table 3; Figure 9 and Table 4), the following performance indicators were computed (Figure 10 and Table 5; Figure 11 and Table 6):

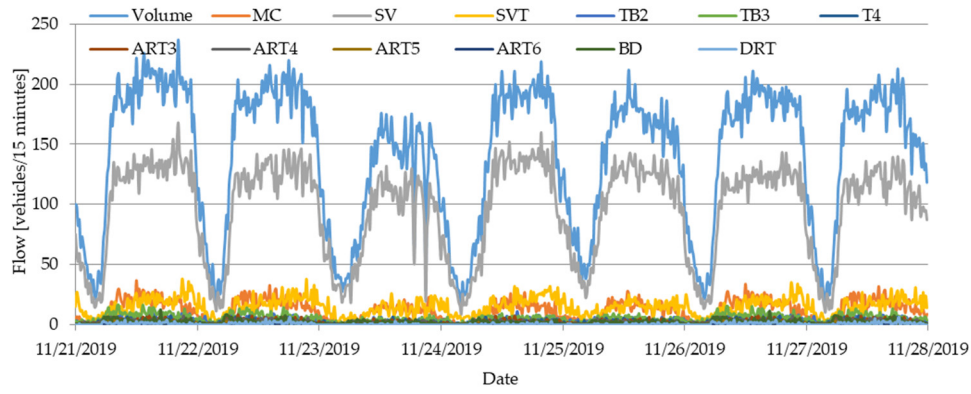
- Vehicular flow (vehicles/15 min).
- Total daily flow (vehicles/day).
- Average speed (km/h).
- 15th percentile speed (v15).
- 85th percentile speed (v85).
- Standard deviation of speed.
- Coefficient of variation of traffic flow.



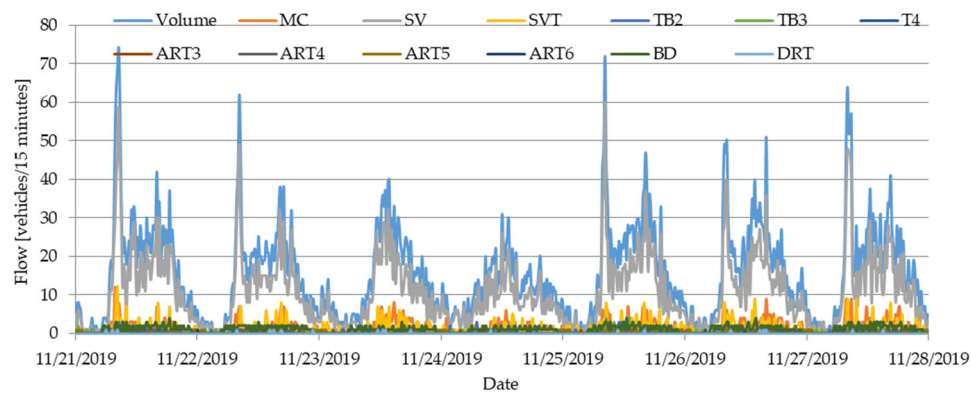
(a)



(b)



(c)

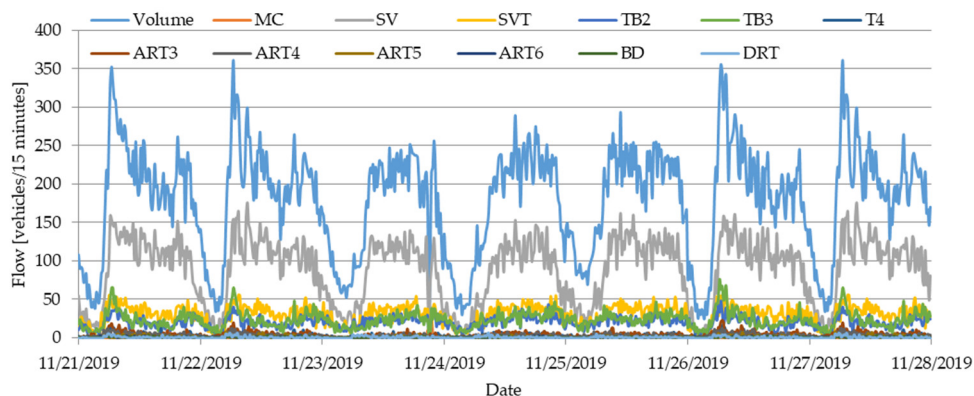


(d)

Figure 8. Traffic flow at the entrance to Lucian Blaga Square (2019): (a) Clinicilor Street, (b) Victor Babeș Street, (c) Petru Maior Street, (d) Gheorghe Șincai Street.

Table 3. Traffic flow at the entrance to Lucian Blaga Square (2019).

| Date | Traffic flow (vehicles / day – every 15 minute by one hour) | | | | Sum (Σ) |
|------------|---|----------|----------|-------------|------------------|
| | Clinicilor | V. Babeș | P. Maior | Ghe. Șincai | |
| 11/21/2019 | 15485 | 11851 | 15119 | 1695 | 44150 |
| 11/22/2019 | 14792 | 10968 | 14651 | 1412 | 41823 |
| 11/23/2019 | 11438 | 7730 | 10726 | 1322 | 31216 |
| 11/24/2019 | 10222 | 6864 | 12985 | 1118 | 31189 |
| 11/25/2019 | 15741 | 11633 | 13221 | 1662 | 42257 |
| 11/26/2019 | 13761 | 12059 | 14067 | 1551 | 41438 |
| 11/27/2019 | 14710 | 12000 | 13618 | 1595 | 41923 |



(a)

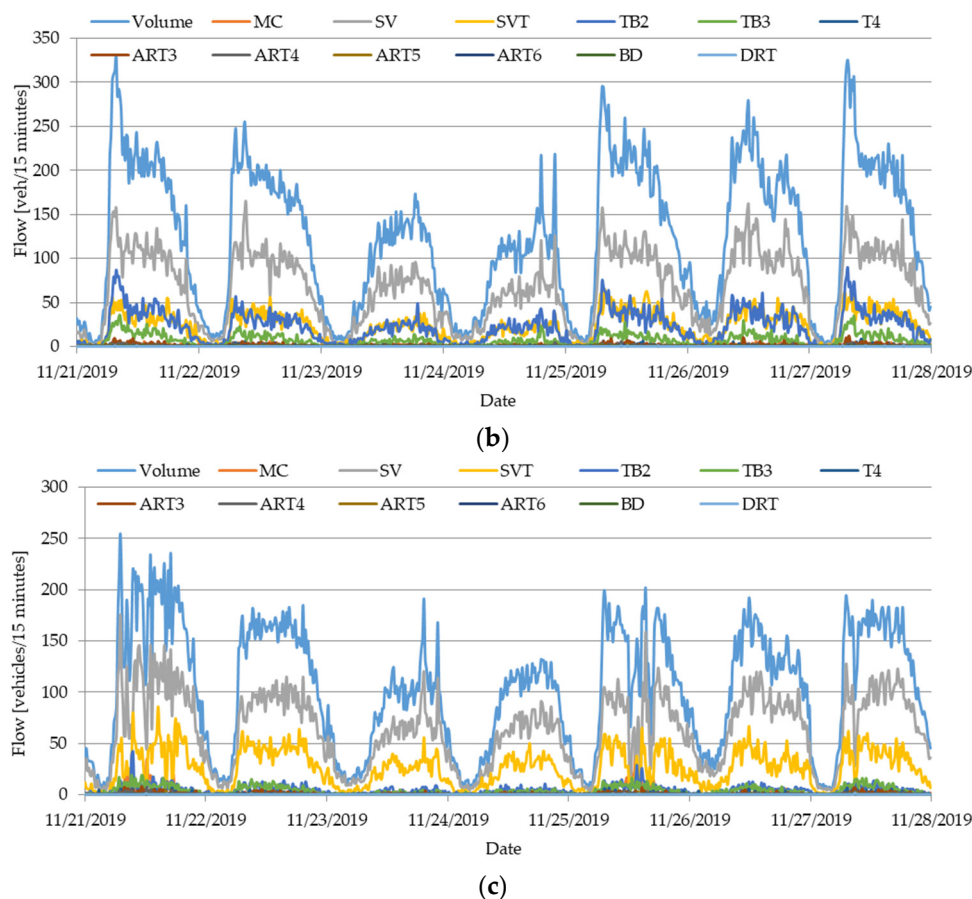


Figure 9. Traffic flow at the exit of Lucian Blaga Square (2019): (a) Petru Maior Street, (b) Napoca Street, (c) Republicii Street.

Table 4. Traffic flow at the exit to Lucian Blaga Square (2019).

| Date | Traffic flow (vehicles / day – every 15 minute by one hour) | | | Sum (Σ) |
|------------|---|--------|------------|------------------|
| | P. Maior | Napoca | Republicii | |
| 11/21/2019 | 17795 | 13914 | 12355 | 44064 |
| 11/22/2019 | 17840 | 12802 | 11121 | 41763 |
| 11/23/2019 | 15686 | 8092 | 7086 | 30864 |
| 11/24/2019 | 16013 | 7871 | 7134 | 31018 |
| 11/25/2019 | 17897 | 13974 | 10435 | 42306 |
| 11/26/2019 | 17347 | 13828 | 10270 | 41445 |
| 11/27/2019 | 17840 | 13671 | 10697 | 42208 |

The daily traffic volumes recorded during 21–27 November 2019 indicate a cumulative total of 273,996 vehicles at the intersection entries and 273,668 vehicles at the exits. The relative difference of 0.12% confirms measurement consistency and appropriate sensor positioning. This minor discrepancy is attributed to vehicles accessing or exiting the nearby underground parking facility and does not indicate detection losses.

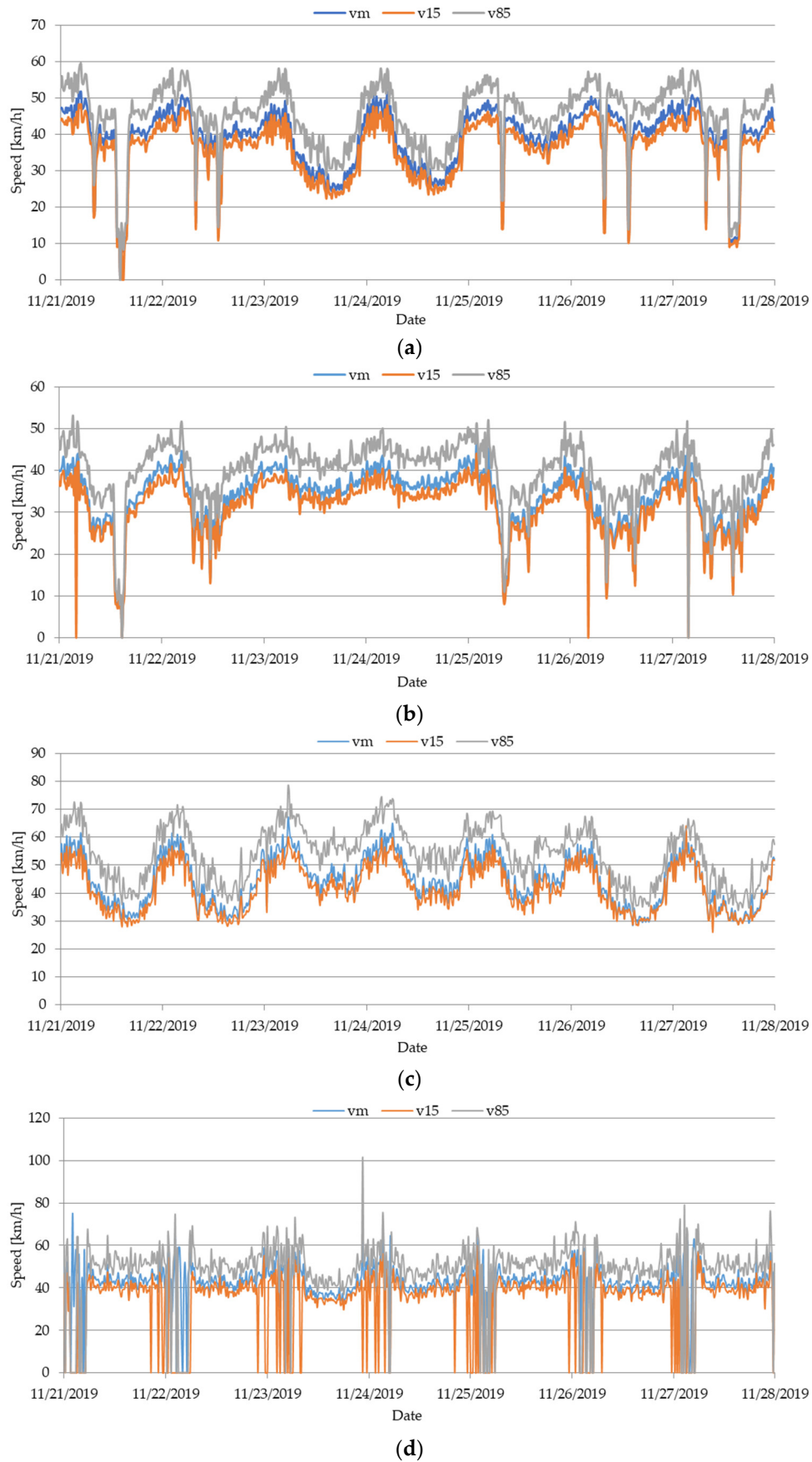
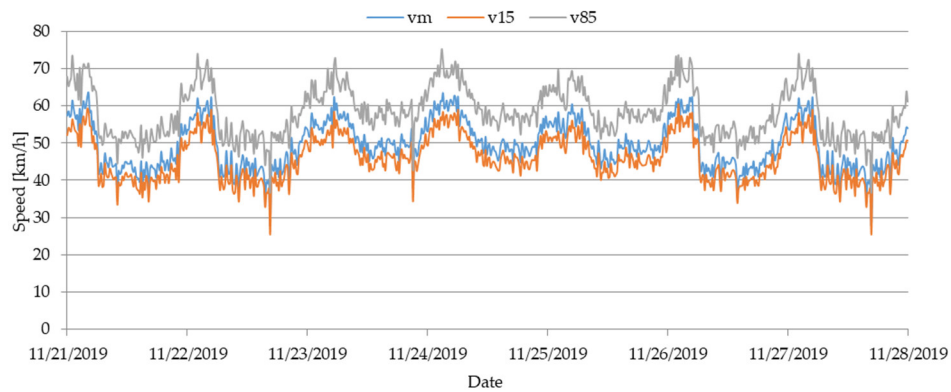


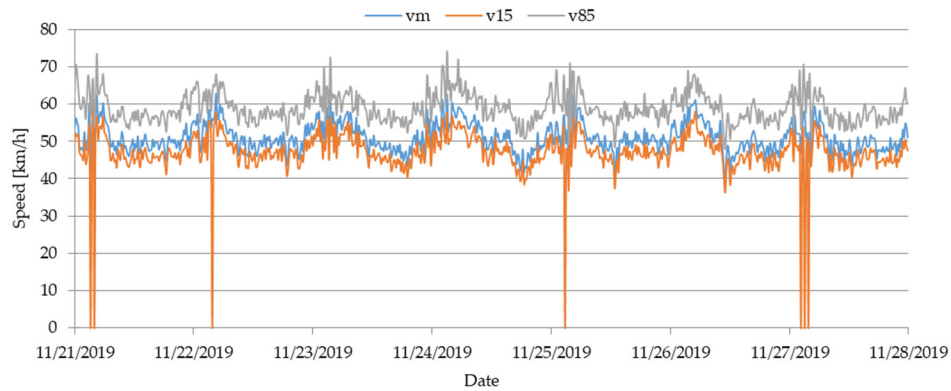
Figure 10. Average traffic speed at the entrance to Lucian Blaga Square (2019): (a) Clinicilor Street, (b) Victor Babeș Street, (c) Petru Maior Street, (d) Gheorghe Șincai Street.

Table 5. Average traffic speed at the entrance to Lucian Blaga Square (2019).

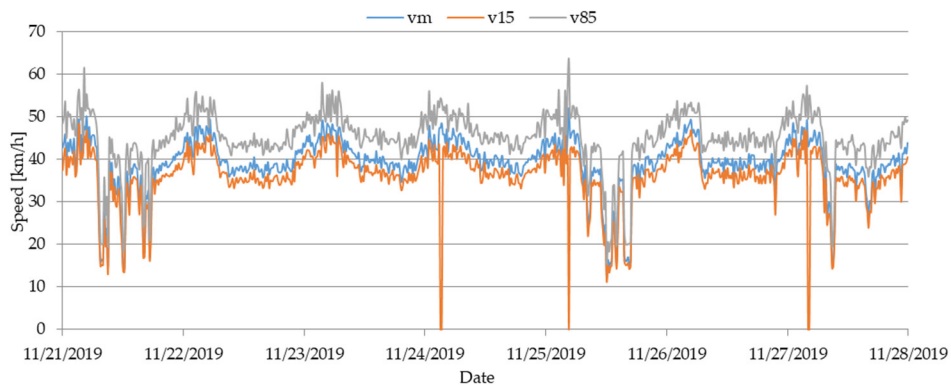
| Date | Average traffic speed (km/h) | | | | Average (km/h) |
|------------|------------------------------|----------|----------|-------------|----------------|
| | Clinicilor | V. Babeş | P. Maior | Ghe. Şincai | |
| 11/21/2019 | 39.43 | 30.48 | 39.61 | 43.51 | 38.26 |
| 11/22/2019 | 39.27 | 30.97 | 39.51 | 42.94 | 38.17 |
| 11/23/2019 | 31.72 | 36.41 | 47.41 | 39.29 | 38.71 |
| 11/24/2019 | 33.33 | 37.86 | 45.37 | 42.10 | 39.67 |
| 11/25/2019 | 40.49 | 29.48 | 45.43 | 43.72 | 39.78 |
| 11/26/2019 | 41.70 | 28.45 | 37.62 | 41.84 | 37.40 |
| 11/27/2019 | 39.34 | 27.52 | 37.40 | 42.92 | 36.80 |



(a)



(b)



(c)

Figure 11. Average traffic speed at the exit of Lucian Blaga Square (2019): (a) Petru Maior Street, (b) Napoca Street, (c) Republicii Street.

Table 6. Average traffic speed at exit from Lucian Blaga Square (2019).

| Date | Average traffic speed (km/h) | | | Average (km/h) |
|------------|------------------------------|--------|------------|----------------|
| | P. Maior | Napoca | Republicii | |
| 11/21/2019 | 45.79 | 49.66 | 33.70 | 43.05 |
| 11/22/2019 | 45.37 | 50.15 | 38.72 | 44.75 |
| 11/23/2019 | 51.05 | 49.56 | 39.82 | 46.81 |
| 11/24/2019 | 50.88 | 49.64 | 39.90 | 46.81 |
| 11/25/2019 | 49.78 | 50.05 | 33.82 | 44.55 |
| 11/26/2019 | 46.32 | 49.27 | 39.49 | 45.03 |
| 11/27/2019 | 45.37 | 49.12 | 36.19 | 43.56 |

The 15-minute aggregated analysis highlights pronounced diurnal variations in traffic flow, with two distinct peak periods corresponding to morning and afternoon commuting hours. An increased coefficient of variation was observed during transition intervals between free-flow and congested regimes, indicating heightened instability in traffic conditions during these intermediate phases.

Average speed values, together with the 15th (v15) and 85th (v85) percentile speeds, confirm the presence of a mixed traffic regime. During low-demand intervals, traffic operated under predominantly free-flow conditions, whereas peak hours exhibited a saturated regime characterized by reduced speeds and increased dispersion.

Video recordings from the fixed surveillance cameras located at Lucian Blaga Square were processed using the DFS Viewer utility to determine the daily traffic distribution for the analyzed approaches (Figure 11).

**Figure 11.** Traffic detection using DFS Viewer (photo by the author).

Table 7 presents a summary of the data obtained from the processing of video recordings.

Table 7. Traffic values 2019 – DFS measurement.

| Daily overview | |
|-----------------------|-------------|
| Date | 23.11.2019 |
| Start time | 8:45:00 |
| End time | 8:50:00 |
| Total period | 00:05:00 |
| Location | Cluj-Napoca |
| Analysis minor period | 05:00 |

| | |
|--|----------------------------|
| Analysis major period | 30:00 |
| Analysis overall period | Disable |
| Intersection type | Traffic light intersection |
| | Overall statistics |
| Number of tracked objects | 425 |
| Vehicle count | 272 |
| Medium vehicle count | 0 |
| Heavy vehicle count | 0 |
| Bus count | 0 |
| Motorcycle count | 1 |
| Bicycle count | 0 |
| Pedestrian count | 140 |
| Light truck count | 1 |
| Van count | 10 |
| Medium truck count | 1 |
| Total distance traveled (px) | 148671.68 |
| Average speed in analyzed area (kpx/h) | 68.72 |

To assess the consistency between the two measurement methods, traffic flows obtained from radar detection and video processing were compared for synchronized 5-minute intervals. The average discrepancy between the two systems was approximately 9%.

This difference can be attributed to technological and operational characteristics of the detection systems. First, the detection domains differ substantially: the radar operates on a defined cross-sectional detection line, whereas the video system captures a two-dimensional observation area. Second, object occlusion and overlapping trajectories may introduce counting inaccuracies in video-based detection. Additionally, objects located near the boundaries of the camera field of view may be affected by geometric distortions or partial information loss, further contributing to the observed deviations.

The traffic flow values aggregated at 15-minute intervals were used to estimate the Poisson parameter λ for each entry and exit branch.

The 2019 dataset defines the baseline traffic regime and serves as the reference condition for evaluating the changes observed in 2020, thereby enabling the assessment of the suitability of the Poisson distribution under different demand levels.

3.2.3. Traffic Measurements (Year 2020)

The measurements corresponding to the lockdown period (April 2020) were conducted using the same methodological framework applied in 2019, ensuring direct comparability of results. Specifically, continuous radar-based measurements (SDR Data Collect) were complemented by video processing through the Data From Sky (DFS) platform. Data aggregation was performed at 15-minute intervals, maintaining the temporal resolution adopted for the reference year.

Table 8 presents an example of video-based measurements for a representative interval (07 April 2020, 08:50–08:55), used to validate object detection and classification accuracy.

Table 8. Traffic values 2020 – DFS measurement.

| Daily overview | |
|-----------------------|-------------|
| Date | 07.04.2020 |
| Start time | 8:50:00 |
| End time | 8:55:01 |
| Total period | 00:05:01 |
| Location | Cluj-Napoca |
| Analysis minor period | 05:01 |

| | | 30:00 |
|--|--|----------------------------|
| | | Disable |
| | | Traffic light intersection |
| Overall statistics | | |
| Analysis major period | | 30:00 |
| Analysis overall period | | Disable |
| Intersection type | | Traffic light intersection |
| Number of tracked objects | | 41 |
| Vehicle count | | 28 |
| Medium vehicle count | | 0 |
| Heavy vehicle count | | 0 |
| Bus count | | 0 |
| Motorcycle count | | 0 |
| Bicycle count | | 0 |
| Pedestrian count | | 7 |
| Light truck count | | 0 |
| Van count | | 5 |
| Medium truck count | | 1 |
| Total distance traveled (px) | | 12577.73 |
| Average speed in analyzed area (kpx/h) | | 36.27 |

The aggregated radar-based traffic flows recorded during April 2020 indicate a substantial reduction in daily traffic volume, reaching an average of 9.55% of the mean daily value observed in November 2019.

The reduction ratio was calculated as:

$$R = \frac{Q_{2020}}{Q_{2019}} \cdot 100\% \quad (4)$$

where: Q_{2020} represents the mean daily traffic flow during the lockdown period and Q_{2019} denotes the corresponding mean daily flow during the reference period.

This result reflects an extremely low-demand traffic regime characterized by the disappearance of conventional peak-hour patterns and a flattened diurnal distribution. Furthermore, a significant decrease in flow variability was observed, accompanied by increased stability of average speeds, indicating operating conditions approaching free flow with minimal vehicle interactions.

Since the availability of video recordings for 2020 was limited to short time windows, the reconstruction of the full daily traffic profile was based primarily on continuous radar measurements.

For the statistical characterization of vehicle arrivals, the 15-minute aggregated flow values were used to estimate the Poisson parameter λ , following the same estimation procedure applied for the 2019 dataset.

3.2.4. The Mathematical Model for Traffic Distribution

To analyze vehicle arrival patterns under the mobility restrictions imposed in 2020, a probabilistic framework based on the Poisson distribution was adopted. The Poisson model is appropriate for arrival-type stochastic processes characterized by discrete, independent events occurring within a finite time interval.

The fundamental assumptions of the model are:

- i. Vehicle arrivals within sufficiently short time intervals are statistically independent.
- ii. The probability of more than one arrival within an infinitesimal interval is negligible.
- iii. The expected arrival rate remains constant within each aggregation interval.

The Poisson probability mass function is defined as:

$$P(n, t) = \frac{(\lambda \cdot t)^n \cdot e^{-\lambda \cdot t}}{n!} \quad (5)$$

where: $P(n, t)$ represents the probability of observing exactly n vehicles within time interval t , λ denotes the mean arrival rate (vehicles per unit time), n is the observed vehicle count and t corresponds to the aggregation interval (15 minutes).

The arrival rate parameter λ was estimated separately for each 15-minute interval using experimental radar measurements from April 2020 [55]:

$$\lambda_i = \frac{q_i}{t} \quad (6)$$

where: q_i represents the observed vehicle count within interval i . Accordingly, the process is treated as a non-homogeneous Poisson process, with a time-varying arrival rate reflecting diurnal traffic dynamics.

Preliminary variance analysis indicated slight overdispersion $var(n) > E(n)$. To assess model robustness, a negative binomial formulation was tested as an alternative count model. The generalized log-linear specification of the arrival rate is:

$$P(n_i) = \prod_i \frac{\exp[-\exp(\alpha_i \beta)] [\exp(\alpha_i \beta)^{n_i}]}{n_i!} \quad (7)$$

To explicitly address overdispersion, a stochastic error component ε_i was introduced:

$$\lambda_i = \exp(\alpha_i \beta + \varepsilon_i) \quad (8)$$

Conditional on ε_i the probability mass function becomes:

$$P(n_i | \varepsilon) = \frac{\exp[-\lambda_i \exp(\varepsilon_i)] [\lambda_i \exp(\varepsilon_i)^{n_i}]}{n_i!} \quad (9)$$

Integrating over the gamma-distributed error term yields the negative binomial distribution:

$$P(n_i) = \frac{\Gamma(\theta + n_i)}{\Gamma(\theta) n_i!} u_i^\theta (1 - u_i)^{n_i} \quad (10)$$

where: $\Gamma(\cdot)$ denotes the gamma function and $u_i = \theta / (\theta + \lambda_i)$, and $\theta = 1/\alpha$ is the dispersion parameter.

Model parameters were estimated using maximum likelihood:

$$P_{max}(\lambda_i) = \prod_{i=1}^n \frac{\Gamma(\theta + n_i)}{\Gamma(\theta) n_i!} \left[\frac{\theta}{\theta + \lambda_i} \right]^\theta \left[\frac{\lambda_i}{\theta + \lambda_i} \right]^{n_i} \quad (11)$$

Goodness-of-fit tests indicated that the Poisson model provides a satisfactory approximation for the analyzed intervals; therefore, the final estimation framework is based on the Poisson distribution.

Video-based observations from 2020 covered only limited time windows. The 2019 dataset, consisting of continuous 24-hour measurements aggregated at 15-minute intervals, was used as a structural reference.

Given that uniform traffic conditions within 15-minute samples were confirmed through DFS-based analysis, the corresponding 5-minute equivalent flow was derived as:

$$q_{unit} = \frac{q_{15}}{3} \quad (12)$$

where q_{15} represents the 15-minute aggregated flow.

The parameter λ was calculated using observations for the data recorded in 2020. Given the data provided in equation 5, the probability that vehicles arrive in a time interval was calculated (Figure 12).

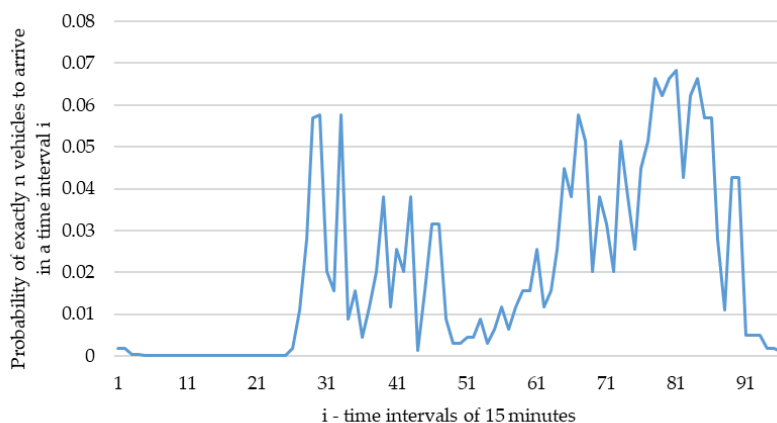


Figure 12. The probability of vehicles arriving in a time interval.

Since the 2020 video data covered short observation windows, the estimated probabilistic model was used to reconstruct the full daily traffic profile:

$$q_i^{2020} = \lambda_i \cdot t \quad (13)$$

where: q_i^{2020} denotes the estimated traffic flow for interval i , and λ_i is the corresponding estimated arrival rate. This formulation preserves dimensional consistency and maintains the physical interpretation of traffic flow as the expected value of the Poisson process.

The index i corresponds to 15-minute intervals for both measured (2019) and estimated (2020) datasets. To reflect the legally imposed night-time traffic restrictions during lockdown (22:00–06:00), the corresponding probability values $P(t)$ were set to zero for these intervals (Figure 13). Notably, 2019 measurements during the same period already exhibited minimal traffic volumes.

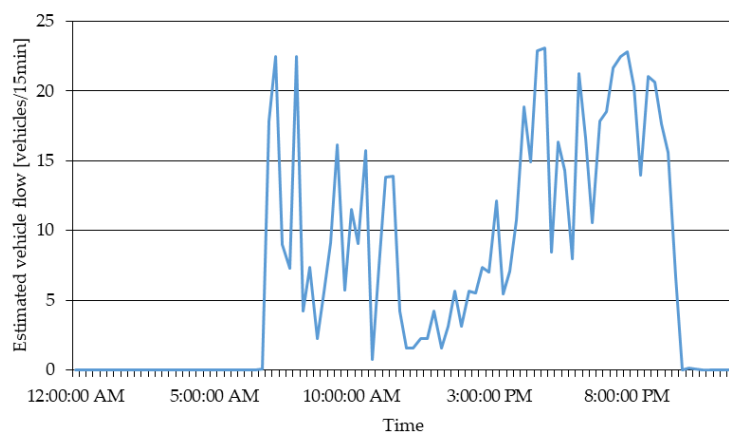


Figure 13. Vehicles traffic at 15-minute interval in 2020.

The reconstructed 24-hour traffic profile was validated using NCSS Statistical Software [56]. The goodness-of-fit analysis yielded a probability level of 0.98, confirming strong agreement between observed and modeled vehicle counts (Figure 14).

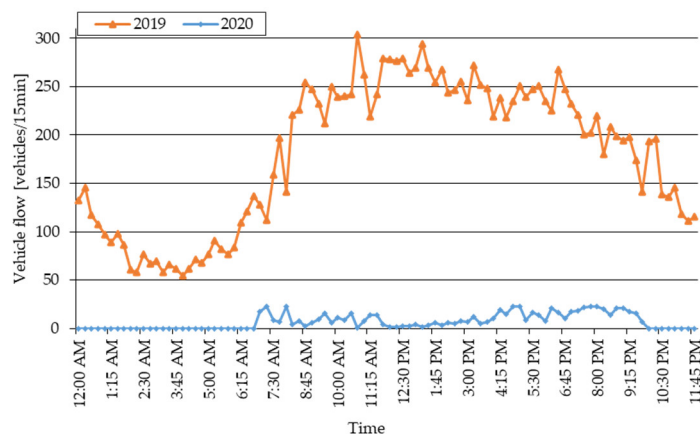


Figure 14. Comparative results: traffic flow distribution over 24 hours.

Comparison of the estimated daily profiles for 2019 and 2020 reveals:

- a pronounced reduction in overall traffic intensity,
- attenuation of traditional morning and afternoon peaks,
- substantial flattening of the diurnal distribution,
- structural modification of temporal demand patterns.

These findings indicate a redistribution of mobility demand across the day and a significant reduction in traffic concentration during conventional peak periods.

The proposed modeling framework enables estimation of traffic behavior under severe mobility restrictions using limited observational data, offering a transferable tool for analyzing extreme mobility scenarios and supporting resilience-oriented urban traffic planning.

4. Results

4.1. Traffic Flow Characteristics Before the Pandemic (2019)

Continuous measurements conducted in November 2019 indicate that traffic at Lucian Blaga Square operated under recurrent high-volume conditions, particularly during peak periods.

The cumulative inflow over the seven monitored days (Figure 8, Table 3) reached 273,996 vehicles, while the cumulative outflow (Figure 9, Table 4) was 273,668 vehicles, corresponding to a relative difference of only 0.12%. This negligible imbalance confirms global flow conservation within the intersection and validates the consistency of sensor positioning and data acquisition.

The average daily inflow was approximately 39,142 vehicles/day, ranging between 31,189 and 44,150 vehicles/day. The corresponding average daily outflow was 39,095 vehicles/day, indicating an almost symmetric distribution of traffic volumes. The coefficient of variation of daily volumes (11–13%) reflects moderate variability, typical of central urban areas characterized by mixed land use (administrative, medical, academic).

The highest daily inflow (44,150 vehicles/day) was recorded on 21 November 2019, corresponding to a regular working day with intense urban activity.

Mean entry speeds (Figure 10, Table 5) ranged between 36.80 and 39.78 km/h, whereas mean exit speeds (Figure 11, Table 6) varied between 43.05 and 46.81 km/h. The average difference of approximately 7–8 km/h between entry and exit speeds reflects the dynamic processes governing intersection operation. Vehicle deceleration and queue formation upstream of the stop line reduces entry speeds, while downstream acceleration and flow dispersion increase exit speeds. This difference is further influenced by the adaptive signal control system, which modulates green times and temporally redistributes traffic demand.

Peak intervals were characterized by inflows reaching 220–250 vehicles per 15-minute interval on major approaches, accompanied by mean speeds dropping below 35 km/h, indicating operation close to saturation conditions.

The combined analysis of flow and speed reveals a clear inverse relationship between traffic intensity and mean speed, consistent with the fundamental diagram of traffic flow (flow–density–speed relationship). Increased demand during peak hours leads to reduced speeds and higher dispersion, confirming the presence of congestion dynamics.

Overall, the 2019 dataset reflects an urban traffic system operating in a dynamic equilibrium state, characterized by high and recurrent volumes, predictable temporal variability, and systematic queue formation during peak periods. This operational regime defines the baseline reference condition for subsequent comparison with the pandemic period.

4.2. Traffic Conditions During COVID-19 Restrictions (2020)

Traffic measurements conducted in April 2020, during the state of emergency, revealed a pronounced structural reduction in mobility demand at the analyzed intersection.

AI-assisted video processing detected 28 vehicles and 7 pedestrians within a representative 5-minute interval. When compared with the equivalent reference period in 2019, these values correspond to approximately 9.55% of the pre-pandemic vehicular traffic and approximately 5% of the pedestrian activity level. This magnitude of reduction confirms a near-collapse of regular urban mobility patterns during lockdown conditions.

Despite the drastic decrease in traffic volumes, the mean vehicle speed recorded during the analyzed interval in 2020 was 36.27 km/h, a value comparable to the entry speed observed under normal conditions. The absence of a proportional increase in speed indicates that traffic performance remained structurally constrained by signal timing and intersection control logic rather than by demand levels alone.

This behavior suggests that, under extremely low demand, the operational regime transitioned from demand-driven congestion to control-driven regulation. In other words, intersection performance during lockdown was governed predominantly by signal coordination parameters rather than by vehicle interactions, confirming a shift toward a quasi-free-flow regime constrained by fixed or adaptive signal cycles.

4.3. Probabilistic Modeling of Vehicle Arrivals

The Poisson distribution was employed to model vehicle arrivals at the intersection during the state of emergency, treating arrivals as a discrete time-dependent stochastic process. The model was formulated as a non-homogeneous Poisson process, with the arrival rate λ_i estimated separately for each 15-minute interval based on the experimental data collected in April 2020.

The estimated values of λ_i ranged between 0 and 1.6 vehicles/min during active daytime periods, with a daily average of 0.42 vehicles/min, corresponding to approximately 25 vehicles per 15-minute interval. These values reflect a severely reduced demand regime compared to the 2019 baseline.

The Poisson probability mass function was used to compute the likelihood of observing n vehicles within a given time interval t .

The variance-to-mean ratio for the 2020 dataset was close to unity ($var(n)/E(n) \approx 1.08$), indicating minimal deviation from the equidispersion property characteristic of Poisson processes.

A chi-square goodness-of-fit test yielded a significance level of $p = 0.98$, confirming that the Poisson distribution adequately describes the arrival process under restricted traffic conditions. To assess potential overdispersion, a negative binomial formulation was also tested. Maximum likelihood estimation of the dispersion parameter α produced values approaching zero ($\alpha \rightarrow 0$), indicating that overdispersion effects were negligible in the low-demand regime.

Consequently, the Poisson model was considered sufficient for reconstructing the daily traffic profile.

Using the estimated λ_i values, the 2020 daily traffic curve was reconstructed. The resulting profile reveals an almost complete suppression of the morning peak (07:00–09:00) and a pronounced attenuation of the afternoon peak (16:00–18:00). Overall, the diurnal variation appears substantially flattened, indicating a redistribution and homogenization of mobility demand throughout the day. Traffic volumes between 22:00 and 06:00 approached zero, consistent with the mobility restrictions in force during the analyzed period.

Compared to 2019, peak-hour flow rates decreased by approximately 88–92%, depending on the approach, while the average daily flow dropped to approximately 9–12% of pre-pandemic levels. These results confirm a structural transition from a peak-dominated regime to a uniformly low-intensity arrival process, statistically compatible with a near-ideal Poisson behavior.

4.4. Model Validation

Statistical validation of the probabilistic framework was performed using NCSS Statistical Software [56], applying the chi-square (χ^2) goodness-of-fit test to evaluate the agreement between observed and Poisson-estimated frequencies.

The calculated χ^2 statistic was lower than the critical value at a significance level of $\alpha = 0.05$, with a reported p-value of 0.98. Therefore, the null hypothesis—that the data follow a Poisson distribution—cannot be rejected. The high p-value indicates excellent agreement between the theoretical model and the empirical observations, confirming that vehicle arrivals during the restriction period are statistically consistent with a Poisson process. Further validation was conducted using the variance-to-mean ratio. For the analyzed intervals, this ratio was approximately 1.08, closely aligned with the equidispersion property of the Poisson distribution. In contrast, peak-hour data from 2019 exhibited variance-to-mean ratios exceeding 1.4, reflecting overdispersion induced by congestion effects and vehicle platooning.

The near-unit dispersion observed in 2020 suggests that, under severely reduced demand, inter-vehicle dependence and platooning effects are substantially diminished. As a result, the independence assumption underlying the Poisson process becomes more realistic compared to normal traffic conditions.

A comparative assessment between 2019 and 2020 is summarized in Table 9.

Table 9. Comparative assessment between 2019 and 2020.

| Indicator | 2019 | 2020 | Change |
|------------------------------|-------------------------|-----------------------|-----------------------|
| Average daily traffic volume | ~39,142 vehicles/day | ~3,740 vehicles/day | −90.4% |
| Peak 15-min flow | 220–250 vehicles/15 min | 18–25 vehicles/15 min | −88–92% |
| Pedestrian activity | Baseline | ~5% of 2019 | −95% |
| Variance-to-mean ratio | >1.4 (peak hours) | ≈1.08 | Reduced dispersion |
| Traffic regime | Near-capacity | Free-flow dominant | Structural transition |

The results confirm that mobility restrictions imposed in 2020 led to a severe reduction in congestion phenomena, the disappearance of the characteristic bimodal daily traffic profile, and a substantial decrease in temporal variability. Moreover, the statistical behavior of vehicle arrivals became increasingly compatible with the fundamental assumptions of the Poisson model.

This transition reflects a shift from a near-capacity operational regime in 2019—characterized by vehicle interdependence and queue formation—to a low-density, free-flow-dominant regime in 2020, characterized by rare and nearly independent arrival events.

The probabilistic model demonstrates robustness under extremely low-demand conditions and provides a reliable tool for estimating traffic behavior in exceptional mobility scenarios. Given the statistical validation and engineering consistency of the results, the Poisson framework can be

considered adequate for describing vehicle arrival distributions during the analyzed lockdown period.

5. Discussion

5.1. Interpretation of Traffic Reduction Under Mobility Restrictions

The results demonstrate a profound structural disruption of urban mobility patterns during the COVID-19 emergency period. Traffic volumes decreased to approximately 9–12% of the 2019 reference level, while pedestrian activity declined to nearly 5%, indicating an almost complete contraction of routine urban mobility at the analyzed central node.

Compared to international findings reporting reductions between 60% and 90%, the observed 88–92% peak-hour reduction places the studied intersection at the upper bound of global impact levels. This heightened sensitivity can be attributed to the functional characteristics of the location, which include a high concentration of administrative institutions, academic facilities, medical services, and commuter-dominated trip patterns. The closure of institutions and the large-scale adoption of remote work directly suppressed the dominant travel demand components.

Importantly, the elimination of the bimodal peak structure and the flattening of the diurnal distribution indicate that restrictions induced not merely a quantitative reduction in volume, but a structural reorganization of temporal demand patterns. The disappearance of pronounced morning and afternoon peaks reflects the collapse of commuting-driven mobility.

The improved compatibility of 2020 data with the assumptions of the Poisson distribution further supports this structural interpretation. Under near-capacity conditions (2019), vehicle interdependence, queue formation, and platooning introduce correlations that violate independence assumptions. Under extremely low demand (2020), arrivals approximate independent rare events, explaining the superior performance of the Poisson model.

These findings suggest that central urban nodes are highly sensitive to institutional activity patterns and that mobility restrictions can rapidly trigger a transition toward a free-flow dominant regime accompanied by fundamental changes in temporal demand structure. This has direct implications for emergency mobility planning and SUMP-based scenario modeling.

5.2. Traffic Regime Transition and Flow Characteristics

In 2019, the intersection operated close to capacity during peak periods, as indicated by high flow rates and reduced mean speeds. The observed flow–speed relationship is consistent with operation near the descending branch of the fundamental diagram, where increased density leads to speed reduction and congestion onset. The likely volume-to-capacity ratio (v/c) approached unity during peak intervals (07:00–09:00 and 16:00–18:00), resulting in recurrent queue formation and shockwave propagation.

During the 2020 restrictions, peak flows decreased by 88–92%, shifting the system to a fundamentally different operational regime. The v/c ratio fell well below unity, eliminating queue formation mechanisms and significantly reducing vehicle interactions. Temporal variability decreased, and the arrival process became statistically closer to independent random events.

Notably, mean speeds did not increase proportionally to the dramatic demand reduction. This indicates that intersection performance under low demand was constrained primarily by signal control logic rather than capacity limitations. In 2019, traffic dynamics were governed predominantly by demand pressure and vehicle interaction effects. In 2020, system behavior became control-dominated rather than capacity-dominated.

This shift reflects a structural transition in the governing mechanisms of the traffic system—from interaction-driven congestion to regulation-driven flow stabilization.

5.3. Suitability of the Poisson Modeling Framework

The Poisson framework relies on two core assumptions:

1. Statistical independence of arrival events.
2. Equidispersion (variance approximately equal to the mean).

Under normal urban traffic conditions, these assumptions are frequently violated due to platooning, upstream signal coordination, congestion wave propagation, and vehicle interdependence. Such conditions typically generate overdispersion and correlated arrivals.

During the lockdown period, reduced density significantly diminished inter-vehicle interactions. The observed variance-to-mean ratio (≈ 1.08) closely approaches the theoretical Poisson condition. The high χ^2 goodness-of-fit significance level ($p = 0.98$) confirms strong agreement between observed and theoretical distributions.

Testing a negative binomial formulation yielded dispersion parameters approaching zero ($\alpha \rightarrow 0$), indicating negligible overdispersion. Consequently, the Poisson model provides a statistically sufficient and parsimonious description of vehicle arrivals under severely reduced demand.

These results confirm that Poisson-based modeling is particularly appropriate for low-density regimes, nighttime traffic, emergency scenarios, and other rare-event mobility contexts. However, its applicability remains limited under near-capacity or highly coordinated signal conditions.

5.4. Methodological Implications of AI-Based Video Processing

The integration of radar-based detection (SDR) and AI-assisted video processing (DFS platform) enabled multi-source validation of traffic volumes and classifications.

Radar measurements provide precise cross-sectional counts and instantaneous speed estimation, while video-based deep learning detection captures full-scene dynamics, enabling trajectory reconstruction, classification, acceleration estimation, and interaction analysis.

The observed $\sim 9\%$ discrepancy between radar and video measurements reflects methodological differences in detection geometry rather than major systematic error. Radar operates on a defined cross-sectional plane, whereas video detection covers a two-dimensional field with potential edge distortions and occlusion effects. The strong temporal correlation between the two datasets confirms coherent representation of flow dynamics.

The hybrid sensing framework enhances robustness, reduces systematic bias associated with single-sensor approaches, and demonstrates the potential of AI-supported monitoring for probabilistic modeling and operational diagnostics of urban intersections.

5.5. Urban Resilience and Traffic Management Implications

The observed collapse of mobility demand provides insights into urban traffic system resilience. In transport engineering terms, resilience can be defined as the ability of the system to absorb extreme external shocks, maintain operational stability, and recover to its original regime.

Despite a 90% demand reduction, the signalized intersection maintained stable operation without systemic malfunction. Adaptive signal control remained functional under atypical arrival distributions, suggesting robust regulatory logic capable of accommodating extreme demand fluctuations.

The probabilistic framework developed in this study offers practical utility for extreme scenario modeling, emergency mobility planning, resilience testing, and rapid reconstruction of daily traffic profiles from limited observations. Such capability is particularly relevant for sudden disruptions including pandemics, natural disasters, or security-related mobility restrictions.

While the study focuses on a single central intersection, the methodological approach is transferable to other urban nodes provided that:

- i. Baseline reference data are available.
- ii. Low-demand observations exist for comparative calibration.
- iii. Arrival processes remain sufficiently sparse to satisfy probabilistic assumptions.

However, extrapolation to multilane coordinated corridors, high-speed freeway segments, or multimodal hubs must be undertaken cautiously, as different interaction dynamics may invalidate

the independence assumption. Future research should therefore investigate whether similar probabilistic behavior emerges across diverse infrastructure typologies and varying demand structures.

6. Conclusions

This study investigated the impact of COVID-19 mobility restrictions on urban traffic dynamics at a central signalized intersection in Cluj-Napoca, Romania, using an integrated framework combining continuous radar measurements and AI-assisted video processing.

The findings reveal an extreme structural contraction of mobility demand. Vehicle volumes decreased to approximately 9.55% of the pre-pandemic baseline, while pedestrian activity declined to nearly 5%. Beyond this quantitative reduction, a fundamental transformation of the temporal traffic structure was observed, characterized by the disappearance of morning and afternoon peak periods and a pronounced flattening of the diurnal profile.

From an operational perspective, the intersection transitioned from a near-capacity, congestion-prone regime (2019) to a low-density, free-flow dominant regime (2020), governed primarily by signal control logic rather than demand pressure. Despite the dramatic reduction in flow, average speeds did not increase proportionally, confirming the persistent structural influence of signal regulation on performance metrics.

The probabilistic modeling framework based on the Poisson distribution—supplemented by a negative binomial robustness test—demonstrated strong agreement with observed data under reduced demand conditions. The variance-to-mean ratio approaching unity and the high χ^2 goodness-of-fit ($p=0.98$) confirm that, under sparse traffic conditions, vehicle arrivals approximate an independent stochastic process more closely than under congested regimes dominated by inter-vehicle interactions and platooning effects.

The integration of radar detection and AI-based video analytics enabled multi-source validation of traffic volumes and strengthened the robustness of probabilistic parameter estimation. The proposed methodological framework allows reconstruction of daily traffic distributions from limited observational datasets and provides a transferable tool for modeling extreme mobility scenarios and supporting resilience-oriented traffic management strategies.

Overall, the study demonstrates that extreme mobility disruptions modify not only traffic intensity but also the stochastic structure of arrival processes, with direct implications for probabilistic modeling and operational traffic management under low-demand conditions.

Several limitations must be acknowledged.

First, the temporal coverage of 2020 data was restricted to a limited lockdown window. The 24-hour traffic profile was reconstructed through probabilistic extrapolation, which introduces uncertainty.

Second, the reference measurements (November 2019) and lockdown measurements (April 2020) were collected in different seasons. Although seasonal effects in central urban nodes are expected to be moderate, influences related to meteorological conditions and daylight duration cannot be entirely excluded.

Third, the analysis focused on a single signalized urban intersection. While representative of mixed-use central areas, generalization to other infrastructure typologies—such as coordinated arterial corridors, freeway segments, or multimodal hubs—should be undertaken cautiously.

Finally, the adopted approach was predominantly macroscopic. Microscopic trajectory analysis, detailed queue dynamics modeling, and behavioral adaptation assessment were beyond the scope of the present study.

Future research should:

- Assess the applicability of the probabilistic framework across diverse network typologies and operational contexts.
- Investigate post-restriction recovery phases and potential rebound effects in mobility demand.

- Integrate microscopic traffic simulation and dynamic queue modeling to capture fine-scale interaction mechanisms.
- Evaluate the long-term stability of stochastic arrival patterns under hybrid work regimes and evolving mobility behaviors.

Such extensions would further clarify the boundary conditions under which Poisson-based modeling remains valid and enhance its integration into adaptive traffic management and resilience-oriented urban mobility planning.

Author Contributions: Conceptualization, N.F. and C.I.; methodology, N.F. and C.I.; software, N.F.; validation, N.F. and M.D.; formal analysis, C.I.; resources, C.I.; data curation, C.I. and M.D.; writing—original draft preparation, C.I.; writing—review and editing, C.I.; visualization, N.F., C.I. and M.D.; supervision, N.F.; project administration, N.F. All authors have read and agreed to the published version of the manuscript.

Data Availability Statement: Access to the data is available upon request. Access to the data can be requested via e-mail to the corresponding author.

Acknowledgments: This paper and the research behind it would not have been possible without the support of the project Just Streets - Horizon 2020 and Data from Sky system, developed by RCE systems s.r.o. and of Monitoring and Road Safety Department within Cluj-Napoca City – Hall, Romania.

Conflicts of Interest: The authors declare no conflicts of interest.

References

1. Urban mobility strategies during COVID-19 https://www.eiturbanmobility.eu/wp-content/uploads/2021/03/Urban-mobility-strategies-during-COVID-19_long-1.pdf (accessed on 11 February 2026).
2. Pandey, S.; Yadav, B.; Pandey, A.; Tripathi, T.; Khawary, M.; Kant, S.; Tripathi, D. Lessons from SARS-CoV-2 Pandemic: Evolution, Disease Dynamics and Future. *Biology* **2020**, *9*, 141.
3. Nazir, R.; Ali, J.; Rasul, I.; Widemann, E.; Shafiq, S. Eco-Environmental Aspects of COVID-19 Pandemic and Potential Control Strategies. *Int. J. Environ. Res. Public Health* **2021**, *18*, 3488.
4. Lipfert, F.W.; Wyzga, R.E. COVID-19 and the Environment, Review and Analysis. *Environments* **2021**, *8*, 42.
5. Taqi, H.M.M.; Ahmed, H.N.; Paul, S.; Garshasbi, M.; Ali, S.M.; Kabir, G.; Paul, S.K. Strategies to Manage the Impacts of the COVID-19 Pandemic in the Supply Chain: Implications for Improving Economic and Social Sustainability. *Sustainability* **2020**, *12*, 9483.
6. Khalifa, S.A.M.; Swilam, M.M.; El-Wahed, A.A.A.; Du, M.; El-Seedi, H.H.R.; Kai, G.; Masry, S.H.D.; Abdel-Daim, M.M.; Zou, X.; Halabi, M.F.; et al. Beyond the Pandemic: COVID-19 Pandemic Changed the Face of Life. *Int. J. Environ. Res. Public Health* **2021**, *18*, 5645.
7. Muhammad, S.; Long, X.; Salman, M.; COVID-19 pandemic and environmental pollution: A blessing in disguise?, *Science of The Total Environment* **2020**, *728*, 138820.
8. Planul de Mobilitate Urbană Durabilă Cluj-Napoca 2021-2030 (in romanian). Available online: https://files.primariaclujnapoca.ro/2022/02/03/PMUD_Cluj-Napoca.pdf (accessed on 11 February 2026)
9. Sustainable urban mobility planning and monitoring. Available online: https://transport.ec.europa.eu/transport-themes/urban-transport/sustainable-urban-mobility-planning-and-monitoring_en (accessed on 11 February 2026).
10. FY 2022-26 U.S. DOT Strategic Plan and Progress Report. Available online: <https://www.transportation.gov/dot-strategic-plan> (accessed on 29 August 2024).
11. Decretul nr. 195 din 16 martie 2020 (in romanian). Available online: <https://legislatie.just.ro/Public/DetaliiDocumentAfis/223831> (accessed on 18 August 2024).
12. Global carbon emissions rebound close to pre-Covid levels. Available online: <https://globalcarbonbudget.org/global-carbon-emissions-rebound-close-to-pre-covid-levels/> (accessed on 11 February 2026).
13. Nath, D.; Sasikumar, K.; Nath, R.; Chen, W. Factors Affecting COVID-19 Outbreaks across the Globe: Role of Extreme Climate Change. *Sustainability* **2021**, *13*, 3029.

14. Wołowiec, T.; Myroshnychenko, I.; Vakulenko, I.; Bogacki, S.; Wiśniewska, A.M.; Kolosok, S.; Yunger, V. International Impact of COVID-19 on Energy Economics and Environmental Pollution: A Scoping Review. *Energies* **2022**, *15*, 8407.
15. Bulmez, A.M.; Brezeanu, A.-I.; Dragomir, G.; Talabă, O.-M.; Năstase, G. An Analysis of Romania's Energy Strategy: Perspectives and Developments since 2020. *Climate* **2024**, *12*, 101.
16. El-Geneidy, A.; De Vos, J. Transport and COVID-19: where are we now? *Transport Reviews* **2024**, *44*:2, pp. 245-247.
17. Institutul Național de Statistică (in romanian). Available online: <https://insse.ro/cms/files/POCA/Impact-COVID-SNDDR2030.pdf> (accessed on 11 February 2026).
18. Bucsky, P. Modal share changes due to COVID-19: The case of Budapest, *Transportation Research Interdisciplinary Perspectives*, **2020**, *8*, 100141.
19. Politis, I.; Georgiadis, G.; Papadopoulos, E.; Fyrogenis, I.; Nikolaidou, A.; Kopsacheilis, A.; Sdoukopoulos, A.; Verani, E. COVID-19 lockdown measures and travel behavior: The case of Thessaloniki, Greece, *Transportation Research Interdisciplinary Perspectives* **2021**, *10*, 100345.
20. Lockdown movement permit (in romanian). Available online: <https://forma.gov.gr/en/> (accessed on 11 February 2026).
21. Henke, I.; Pagliara, F.; Carteni, A.; Coppola, P. The Impact of COVID-19 Pandemic on Public Transport: A Mobility Survey in Naples (South of Italy), *The Open Transportation Journal* **2023**, *17*.
22. Harantová, V.; Hájnik, A.; Kalašová, A.; Figlus, T. The Effect of the COVID-19 Pandemic on Traffic Flow Characteristics, Emissions Production and Fuel Consumption at a Selected Intersection in Slovakia. *Energies* **2022**, *15*, 2020.
23. Jenelius, E.; Cebecauer, M. Impacts of COVID-19 on public transport ridership in Sweden: Analysis of ticket validations, sales and passenger counts, *Transportation Research Interdisciplinary Perspectives* **2020**, *8*, 100242.
24. Ren, M.; Park, S.; Xu, Y.; Huang, X.; Zou, L.; Wong, M.S.; Koh, S.-Y. Impact of the COVID-19 pandemic on travel behavior: A case study of domestic inbound travelers in Jeju, Korea, *Tourism Management* **2022**, *92*, 104533.
25. Hong, Y.; Lu, K. The effect of quarantine policy on pollution emission and the usage of private transportation in urban areas. *Nature Scientific Reports* **2024**, *14*, 15752.
26. Li, D.; Lasenby, J. Investigating impacts of COVID-19 on urban mobility and emissions, *Cities* **2023**, *135*, 104246.
27. Suzuki Goshima, C.Y.; Dias, V.C.; Pedreira Junior, J.U.; Pitombo, C.S. Relationships between Teleworking and Travel Behavior in the Brazilian COVID-19 Crisis. *Future Transp.* **2023**, *3*, 739-767.
28. Golinska-Dawson, P.; Sethanan, K. Sustainable Urban Freight for Energy-Efficient Smart Cities—Systematic Literature Review. *Energies* **2023**, *16*, 2617.
29. Creutzig, F.; Lohrey, S.; Franza, M.V. Shifting urban mobility patterns due to COVID-19: comparative analysis of implemented urban policies and travel behaviour changes with an assessment of overall GHG emissions implications, *Environmental Research: Infrastructure and Sustainability* **2022**, *2*, 041003.
30. Yadav, S.K.; Akhter, Y. Statistical Modeling for the Prediction of Infectious Disease Dissemination With Special Reference to COVID-19 Spread. *Front. Public Health* **2021**, *9*, 645405.
31. Peköz, E.A.; Joglekar, N. Poisson Traffic Flow in a General Feedback Queue. *Journal of Applied Probability* **2002**, *39*(3), 630–636.
32. Abul-Magd, A.Y.; Modelling highway-traffic headway distributions using Superstatistics. *Physics Review E* **2007**, *76*(5), 057101-1-4.
33. Wigner's Surmise. Available online: https://robertsweeneyblanco.github.io/Computational_Random_Matrix_Theory/Eigenvalues/Wigner_Surmise.html (accessed on 11 February 2026).
34. Maya, O.; Kim, H.; Toda, H. Online Traffic Flow Prediction Using Convolved Bilinear Poisson Regression. 18th IEEE International Conference on Mobile Data Management (MDM) 2017, pp. 134–43.
35. Yang S.; Yang X.; The Application of the Queuing Theory in the Traffic Flow of Intersection, World Academy of Science, Engineering and Technology International Journal of Mathematical, Computational, Physical, Electrical and Computer Engineering, 2014, 8(6), 986-989.

36. Thomas, T.; Weijermars, W.; Berkum, E. Variations in urban traffic volumes. *European Journal of Transport and Infrastructure Research* **2008**, *8*(3), 251-263.
37. Viti, F.; van Zuylen, HJ. Queues and delays at signals: a general approach. In HJ. van Zuylen (Ed.), Proceedings INSTR2007 2007, 1-9.
38. Vandaele, N.; van Woensel, T.; Verbruggen, A. A queueing based traffic flow model, *Transportation Research Part D: Transport and Environment* **2000**, *5*(2), 121-135.
39. Kong, X.; Xu, Z.; Shen, G.; Wang, J.; Yang, Q.; Zhang, B. Urban traffic congestion estimation and prediction based on floating car trajectory data, *Future Generation Computer Systems* **2016**, *61*, 97-107.
40. SDR Traffic Classifier. Available online: <https://traffictchnology.co.uk/blog/portfolio/sdr-traffic-classifier/> (accessed on 11 February 2026).
41. SDR radar traffic classifier. Available online: <https://www.datacollect.com/en/mobility-data-analysis/measuring-systems/sdr-radar-traffic-classifier/> (accessed on 11 February 2026).
42. Preda, I.; Covaciu, D.; Florea, D.; Ciolan, G. Study of In-Traffic Vehicle Behaviour, Based on GPS and Radar Devices, ESFA 2009 International Conference, Bucharest, Romania, January 2009.
43. Data Collect Traffic Systems. Available online: <https://datafromsky.com/trafficcamera/> (accessed 11 February 2026).
44. Chen, V.C., Li, F., Ho, S.-S. and Wechsler, H. Micro-Doppler effect in radar: phenomenon, model, and simulation study. *IEEE Transactions on Aerospace and Electronic Systems* **2006**, *42*/1, 2-21.
45. Chen, V.; *The Micro-Doppler effect in radar*, Second Edition; Publisher: Artech House, 2019.
46. MyTrafficData Secure: configure, analyse and more. Available online: <https://www.datacollect.com/en/mobility-data-analysis/mytrafficdata/> (accessed on 11 February 2026).
47. Data from Sky Light. Available online: <https://ai.datafromsky.com/light/> (accessed on 11 February 2026).
48. Data from Sky. Available online: Aerial <https://ai.datafromsky.com/aerial> (accessed on 11 February 2026).
49. Data from Sky Viewer. Available online: <https://datafromsky.com/news/datafromsky-viewer-new-version-new-features/> (accessed on 11 February 2026).
50. Conteo de flujo y programación de semáforos, mediante el uso de reconocimiento de imágenes, utilizando el software DataFromSky. Available online: <https://repositorio.uchile.cl/handle/2250/184342> (accessed on 11 February 2026).
51. Dell'Acqua, G., & Wegman, F. (Eds.). Transport Infrastructure and Systems: In Proceedings of the AIIT International Congress on Transport Infrastructure and Systems, Rome, Italy, 10-12 April 2017.
52. Cluj-Napoca, Romania Population 2024. Available online: <https://worldpopulationreview.com/cities/romania/cluj-napoca> (accessed on 11 February 2026).
53. Strategia Integrată de Dezvoltare Urbană a Zonei Metropolitane Cluj (in romanian). Available online: <https://documents1.worldbank.org/curated/en/099850010282239359/pdf/P172384038eb760700add008aa9b21cd8bf.pdf> (accessed on 11 February 2026).
54. ARX Classification Vehicles Schemes. Available online: <https://mtehelp.tech-metrocount.com/Article.aspx?id=DB9FE70AC7> (accessed on 11 February 2026).
55. Azimi, M.; Wali, M.M.; Qi, Y. Studying the Impact of the COVID-19 Pandemic on Bikeshares as a Mode of Shared Micromobility in Major Cities: A Case Study of Houston. *Future Transp.* **2024**, *4*, 270-282.
56. NCSS Statistical Software. Available online: <https://www.ncss.com/software/ncss/> (accessed on 11 February 2026).

Disclaimer/Publisher's Note: The statements, opinions and data contained in all publications are solely those of the individual author(s) and contributor(s) and not of MDPI and/or the editor(s). MDPI and/or the editor(s) disclaim responsibility for any injury to people or property resulting from any ideas, methods, instructions or products referred to in the content.